Q. J. R. Meteorol. Soc. (2002), **128**, pp. 1929–1952

Two-dimensional simulation of orographic effects on mesoscale boundary-layer convection

By WEN-SHOU TIAN and DOUGLAS J. PARKER*
University of Leeds, UK

(Received 14 December 2000; revised 14 September 2001)

SUMMARY

In this paper, orographic effects on mesoscale boundary-layer convection are studied through a series of idealized numerical experiments. It is found that hills tend to weaken convective activity at their summits under higher background winds, whilst strong updraughts can be observed at the summits, or slightly downwind of the peaks, under light-wind conditions; these can be associated with so-called convective cores. When the background winds are strong, the effects of the hill length on the results are only significant when the height of the hill reaches 500 m. The combined effect of a sensible-heating maximum on the hill summit and baroclinic tendencies due to the elevated heating is a tendency to produce a convective core under reasonably light-wind conditions. Under higher-wind conditions, the strong ascents and descents on both sides of the hill, as well as the lee-wave dynamics, seem to pose a more important impact on the convective features than the thermal forcing of the hill. A Richardson-number balance has been proposed to explain these two kinds of response. Finally, under stronger-wind conditions, the convective available potential energy (CAPE) is small at the summit and reaches its maximum value in the lee of the hill while, under light-wind conditions, the air parcels at the summit have more buoyancy and the CAPE downwind of the top of the hill is slightly larger than that elsewhere.

KEYWORDS: Convective boundary layer Convective core Numerical simulation

1. INTRODUCTION

A number of observational and numerical studies have noted that high land or mountain areas are frequently marked by enhanced convection and cloud-cluster generation (e.g. Martin and Schrener 1981; Tripoli and Cotton 1989; Rowell and Milford 1993), and have supported the idea that orography may play an important role in the triggering of convection. Some of the previous studies have simulated observed cases of orographically triggered mesoscale deep convection with explicit representation of convection (e.g. Tripoli and Cotton 1988), but without detailed and systematic attempts to describe the terrain-related boundary-layer shallow convection. In recent years, some numerical studies have been carried out to evaluate the impacts of topography on the convective boundary layer (CBL) using large-eddy simulation (LES) (e.g. Walko *et al.* 1992; Gopalakrishnan *et al.* 2000), and the results from these simulations indicate that the impacts of the topography on the CBL are dependent on both the horizontal and the vertical scales of the terrain. Although LES has been thought to be the best and fundamental approach to turbulence modelling, and to be particularly useful for modelling the unstable and convective boundary layer, its application in mesoscale simulations is computationally limited. In most cases, LES is performed over relatively small domains with resolutions ranging from centimetres to one or two hundred metres. Mesoscale simulation, where the horizontal resolution is generally not less than 1 km, precludes any attempts to resolve the turbulent motions and the standard turbulence closure schemes (e.g. first-order closure, 1.5-order closure) are still widely used in many numerical models.

Although some previous studies (e.g. McNider and Pielke 1981; Bader *et al.* 1987; Bader and McKee 1991) have simulated the evolving mesoscale boundary layer over complex terrain using traditional numerical models in association with a standard turbulence closure scheme, there have been relatively few systematic idealized modelling

* Corresponding author: Institute for Atmospheric Science, School of the Environment, University of Leeds, Leeds, LS2 9JT. e-mail: doug@env.leeds.ac.uk

studies of the impacts of the topography on the mesoscale boundary-layer convective features. On the other hand, with the results and the insight provided by the above-mentioned LES simulations of the CBL over relatively small-scale terrain, one may expect to be able to know whether generally similar results can be obtained when a numerical model having standard turbulence closure schemes (rather than LES) is used over relatively large domains, i.e. of the order of 20 km to 100 km.

In the present work, a numerical model is used in association with standard turbulence closure schemes to study the potential influences of orography on mesoscale boundary-layer convective features through a series of idealized numerical experiments. Efforts are made to test the dependence of the simulations on various assumptions. Section 2 describes the numerical model and section 3 outlines the simulation parameters. Section 4 describes results and model diagnostics, while section 5 provides discussion and conclusions.

2. Model description

The primary tool used in this study is a three-dimensional (3D) Boussinesq boundary-layer model, BLASIUS, described by Wood and Mason (1991, 1993). The model is non-hydrostatic and employs the terrain-following coordinate system defined by Clark (1977). The model grid is staggered and uses a non-uniform vertical grid with much higher resolution in the boundary layer. In the current form, the model includes explicit water vapour, but condensation and latent-heat release are not included and humidity is only calculated to correct the virtual temperature and to diagnose convective parameters such as convective available potential energy (CAPE). The inclusion of cloud process in the model is beyond the scope of the present study and will be addressed in future work.

Wood (1995) found good agreement between two-dimensional (2D) simulations using this nonlinear model and theoretical predictions, while Hewer (1998) used this same model to simulate the wind field over a hill of about 100 m high and axisymmetric in shape, and found that the model can give good predictions of the mean wind field when compared with observations. No attempts are made here to test the model's reliability and its ability to predict specific observational cases; rather the model is used to explore the dependence of flow characteristics on controlling parameters.

In the current study, the model has been run in a 2D configuration. Although the assumption of two dimensionality unavoidably imposes some constraints on the real circulation, it is generally justifiable for horizontal convective rolls, which are the most common forms of boundary-layer convection, or the initial mode of shallow boundary-layer convection (Weckwerth *et al.* 1999). The results of the three-dimensional LES simulations by Gopalakrishnan *et al.* (2000) indicated that neither the length nor the height of the hills has an appreciable influence on the time- and space-averaged variance of the velocity field in the y-direction because of topographical homogeneity, while our limited 3D test runs, which were performed over a 40 km $\times$ 10 km horizontal domain with a 2D ridge extending uniformly in the y-direction, also show that the convective features in the y-direction are homogeneous. Apart from the important assumption of two-dimensionality, another uncertainty lies in the representation of turbulence. The use of LES is excluded from the current study, as described above. The 1.5-order closure scheme is generally thought to be better than a first-order mixing-length closure scheme, especially for convective boundary-layer simulations, but our test runs show that the 1.5-order closure scheme gives similar answers to the first-order mixing-length scheme. For computational efficiency, the first-order mixing-length closure has been adopted in

the current study. It should be pointed out that the mixing-length scheme in our model is similar to that employed in three-dimensional LES (e.g. Deardorff 1977), except that the model is run in a two-dimensional configuration and the upper bound to the mixing length, l_0, is prescribed. Mason and Sykes (1982) pointed out that l_0 had an effect on model simulations, and the appropriate approach was to use the observations to determine the dominant scale of small eddies. However, their results, as well as the observations of LeMone (1973), suggest that a choice of around 50 m is a reasonable one. In this work, l_0 is fixed at 50 m.

3. Description of the numerical experiments

A 10 km deep domain is chosen and an artificial Rayleigh damping layer is added to the top half of the model domain so that upward-propagating wave energy is damped to negligible amplitudes to minimize reflection when it reaches the upper boundary. The choice of the domain length is important because the tendency of two-dimensional models to transfer energy (mainly towards low wave numbers) leads to an impact of domain size on the results (Schadler 1990). Mason and Sykes (1982) also found that the length of the domain affects the number of rolls in the simulation domain, and that a bigger domain size results in more rolls, while Moeng and Sullivan (1994) found that a small domain size makes it difficult to determine the roll orientation in 3D simulations. To clarify the extent to which the model domain length affects the results and to determine what the appropriate domain length is for the current study, domains of length 20, 40 and 60 km were tested in several runs at first; the results are discussed in section 4. The mesh is uniformly spaced in the x-direction with a grid space of 1 km. In a high-resolution test run, a grid space of 250 m is used. For all runs, the vertical mesh is stretched and has 50 points.

The boundary conditions imposed around the simulation domain are the following. Lateral boundary conditions are periodic. At the top boundary the vertical velocity is zero, while zero vertical fluxes are assumed for horizontal wind components; a no-slip condition is applied at the lower boundary. The lower boundary conditions for temperature and humidity are supplied by a full energy balance scheme described by Huntingford *et al.* (1998) in which the energy input A from incoming radiation is balanced by sensible- and latent-heat fluxes. The heat fluxes into the model during the simulation can be controlled by changing A and the surface resistance, $r_s(x)$.

All model runs were initialized with results from 1D simulations and the model was integrated forward in time for three hours, by which time an approximately steady-state solution was reached, in which the mean model state was slowly varying relative to the advection time. The time step was initially set to 0.1 s and adjusted by the model according to numerical stability criteria during the model run. The model parameters, which may be varied between different runs, are:

- the maximum height, h, and width, l, of the hill;
- the large-scale geostrophic wind, u_g;
- the energy input, A, into the model and the surface resistence, $r_s(x)$.

For all runs with a hill in the centre of the domain, the hill profile satisfies

$$Z_s(x) = h \cos^2\left(\frac{\pi x}{l}\right). \tag{1}$$

While observational, numerical and theoretical studies have shown that buoyancy, wind speed and vertical wind shear are dominant factors that affect the boundary-layer

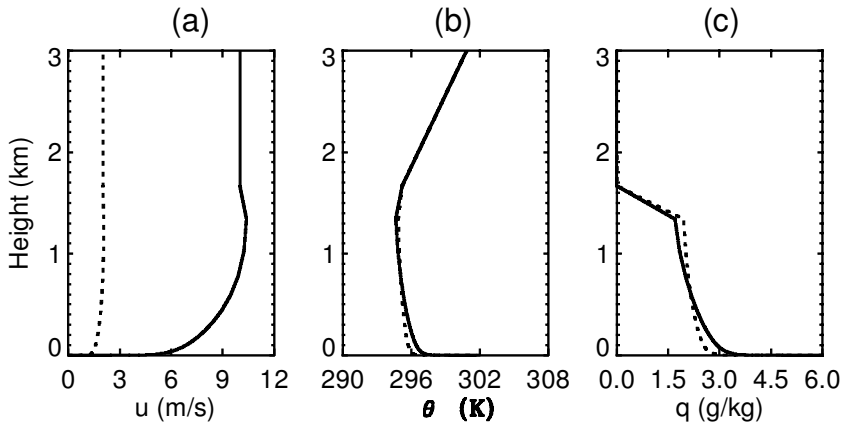

Figure 1. Initial profiles of (a) wind speed, (b) potential temperature and (c) humidity from two one-dimensional runs. Dashed lines and solid lines indicate the results from simulations with geostrophic winds of 2 m s^{-1} and 10 m s^{-1}, respectively.

TABLE 1. MODEL CONFIGURATIONS FOR DIFFERENT RUNS

Configuation	Hill top (m)	Hill width (km)	A (W m^{-2})	u_g (m s^{-1})	$r_s(x)$ (s m^{-1})
A1	100.0	10.0	480.0	10.0	150.0
A2	200.0	10.0	480.0	10.0	150.0
A3	500.0	10.0	480.0	10.0	150.0
A4	500.0	10.0	480.0	10.0	100.0
A5	500.0	10.0	480.0	10.0	1.0×10^9
A6	500.0	10.0	96.0	10.0	1.0×10^9
A7	500.0	10.0	48.0	10.0	1.0×10^9
A8	500.0	10.0	0.0	10.0	1.0×10^9
A9	100.0	20.0	480.0	10.0	150.0
A10	200.0	20.0	480.0	10.0	150.0
A11	500.0	20.0	480.0	10.0	150.0
A12	500.0	20.0	0.0	10.0	1.0×10^9

A is the energy input into the model, u_g is the geostrophic wind, and $r_s(x)$ is the surface resistance.

convective features (e.g. LeMone 1973; Moeng and Sullivan 1994; Weckwerth *et al.* 1997; and many others), we are interested in terrain-related effects under conditions of certain combination of these three factors. Two background wind speeds, u_g, were used in this study, i.e. 2 m s^{-1} and 10 m s^{-1} representing light-wind conditions and stronger-wind conditions, respectively. The results are discussed with respect to different wind conditions in association with different surface energy inputs, but no attempts are made to address the effects of the wind shear on convective features that have been well documented in previous literature.

Figure 1 shows some of the initial fields produced by running the model in 1D with a surface energy input of 480 W m^{-2}, and large-scale geostrophic westerly wind components of 10 m s^{-1} and 2 m s^{-1}, respectively.

The 12 basic configurations used in various runs are listed in Table 1. Twelve other configurations that are used (labelled hereafter as B1–B12) are identical to A1–A12 except that the large-scale geostrophic westerly wind u_g is 2 m s^{-1}. The Coriolis parameter f and the basic state stability N (Brunt–Väisälä frequency) are fixed for all

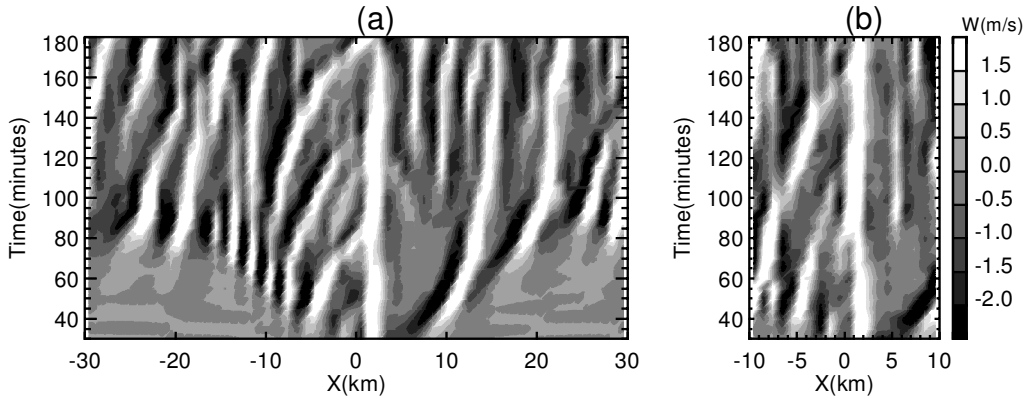

Figure 2. Hovmöller diagrams of the vertical velocity from two runs with domain lengths (a) 60 km, and (b) 20 km. The model configuration for these two runs is B3 (see text). The sections are taken at 600 m above ground level and the whole model domain is shown. The time series was gathered every 5 min, after 30 min of model simulation.

runs with $f = 10^{-4}$ s^{-1} and $N = 0.012$ s^{-1}. The other model parameters not listed in Table 1 have the same values for all runs, unless otherwise stated.

4. Results and diagnostic analysis

(*a*) *Effects of domain length on the results*

Mason and Sykes (1982) tested the effects of domain length on the results from their 2D simulations over flat and relatively small domains and found that the 4 km and 8 km domains gave very similar (and, thus, presumably domain-length independent) results. Here, we first consider three domains of length 20 km, 40 km and 60 km.

The Hovmöller diagrams of vertical velocity from two runs with domain lengths 20 km and 60 km, respectively, (not shown) for model configuration A3 indicate that the characteristics of the convective cells, such as cell spacing and cell size, are not sensitive to the domain length. The time for the model to reach a near steady-state solution is slightly affected by domain length, the larger domain length needing a longer time for the model to reach a quasi-steady state. The same simulations were also produced based on model configuration B3 (light-wind conditions) (Fig. 2). In this case the results over the 20 km domain provide far less information about the modification of eddies passing between a flat surface and a hill than those over the 60 km domain. When a 40 km domain is used, the results are quite similar to those of simulations with a 60 km model domain, and so a 40 km domain is used in all subsequent runs.

Finally, to confirm that the horizontal resolution and the turbulence closure scheme used in this study can produce reasonable convective features, a run with first-order scheme and much higher horizontal resolution (horizontal grid spacing 250 m) and a run with the 1.5 order scheme but the low horizontal resolution (horizontal grid spacing 1 km) were produced. The model configuration for these two runs is A3 and the model domain is 40 km. The Hovmöller diagrams of vertical velocity from these two simulations are depicted in Fig. 3. The solutions are sensitive to the horizontal resolution but are not sensitive to the turbulence closure scheme. In the high-resolution simulation the convective features are more finely resolved and the convective eddies are more intermittent and sporadic. Although the higher horizontal resolution solution is presumably more realistic, the general features are not lost in the low horizontal

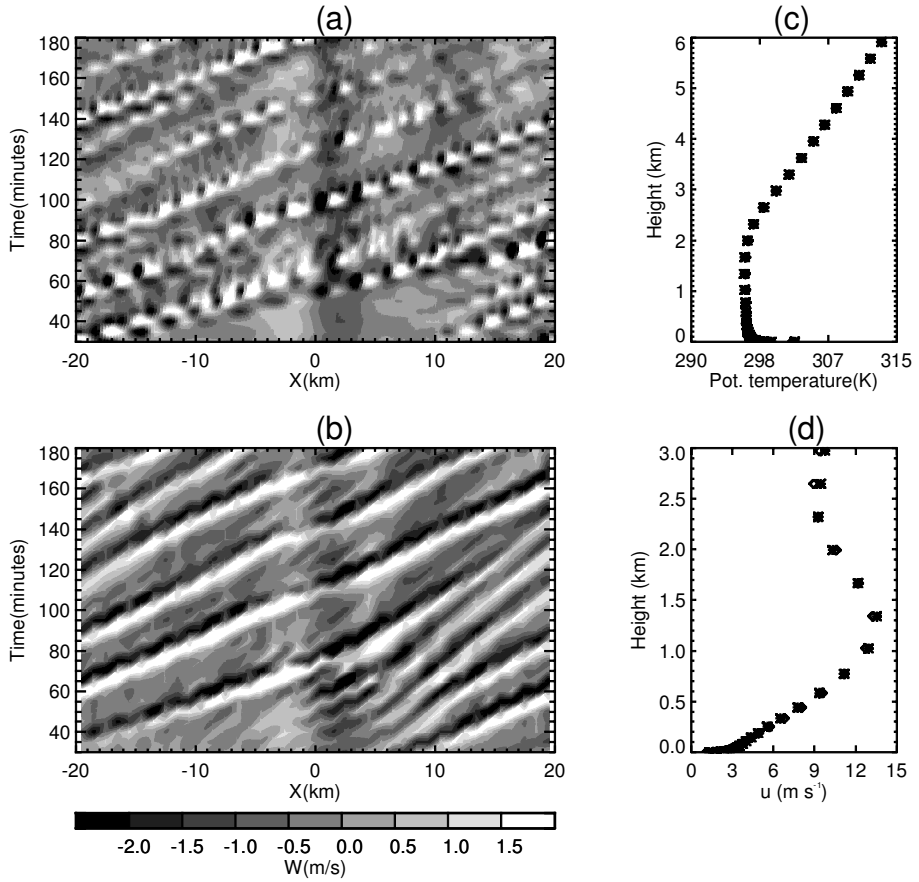

Figure 3. Hovmöller diagrams of vertical velocity from (a) the high-resolution run and (b) the run with the 1.5-order turbulence closure scheme. Both runs were performed over 40 km horizontal domain with model configuration A3 (see text). The section is taken at 600 m above ground level. The vertical profiles of (c) the horizontally averaged potential temperature and (d) the horizontal velocity u at model simulation time 180 min for both simulations are also shown (the high-resolution run is represented by asterisks).

resolution simulations and the mean structure of the temperature and horizontal velocity fields at final stage of the model simulation in both runs is nearly the same.

(*b*) *Effects of the hill on convective features under strong background wind conditions*

Without any perturbation, the model generates no vertical motions over a flat, but uniformly heated, surface. We start all the simulations with a hill located in the model domain to produce perturbations and, hence, to trigger vertical motions.

(i) *Overall features.* The Hovmöller diagrams of vertical velocity from simulations with model configurations A1, A2, A3 and A11 are presented in Fig. 4. It is evident that organized vertical motions develop in all cases with convective motions being first generated downstream of the hill. After about an hour's simulation, the model steady-state solution seems to be reached and linear convective eddies move steadily along the main wind direction with a speed around 6.6 m s^{-1}. Also noticeable is that overall features exhibited in the Hovmöller diagrams of vertical velocity are not significantly influenced by hills with different heights and widths. These convective eddies seem to be

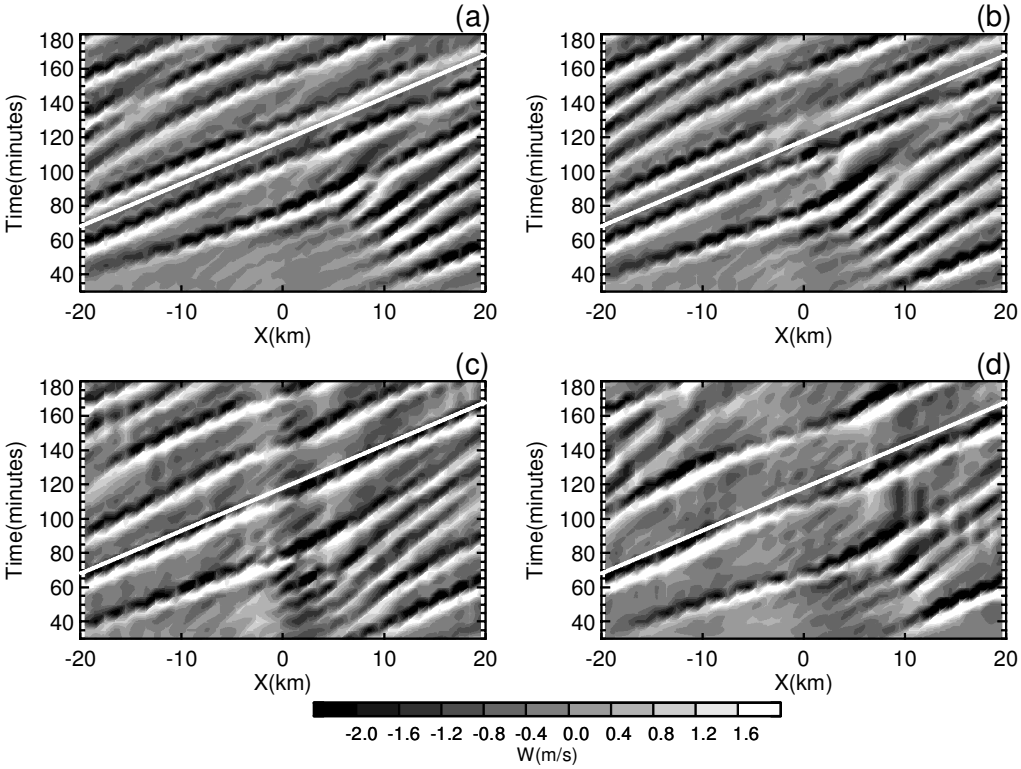

Figure 4. Hovmöller diagrams of vertical velocity from simulations with different model configurations. Panels (a), (b), (c) and (d) correspond to model configurations A1, A2, A3 and A11, respectively (see text). The sections are all taken at 600 m above ground level. The line in each panel represents a speed of 6.6 m s^{-1}.

independent of the hills when they have reached steady state, and the hills tend to disturb them, rather than destroy them or create new ones, because the hills are significantly shallower than the boundary-layer and eddy depths.

A comparison between Fig. 4(d) and Figs. 4(a), (b) and (c) reveals that the hill width forces more significant differences in convective features than the hill height. When the hill has a width and a height of 20 km and 500 m, respectively, there are fewer convective eddies in the simulation domain and some of them are too weak to persist over the hill (Fig. 4(d)), while there are at least four steadily propagating convective eddies in the domain when hill has a width of 10 km (Figs. 4(a), (b) and (c)). However, the simulations with model configurations A9 and A10 (not shown) exhibit no significant differences in their results when compared with the simulations with model configurations A1 and A2. This suggests that, when the hill reaches a certain height, the length of the hill has a significant impact on the convective features while, below that height, different hill lengths make only small differences in the CBL features. This is consistent with the results of the LES simulations by Gopalakrishnan *et al.* (2000), which indicate that the higher the hills, the stronger the impact of the hill length on the CBL properties.

The signature of the terrain-related vertical motions can be noted from Figs. 4(b), (c) and (d). To see this more clearly, Fig. 5 shows the Hovmöller diagram of vertical velocity from the run with model configuration A8. Without surface heating the convective eddies disappear, but vertical motion generated solely by the terrain is evident. The forced ascent on the windward slope can be detected throughout the simulation, while

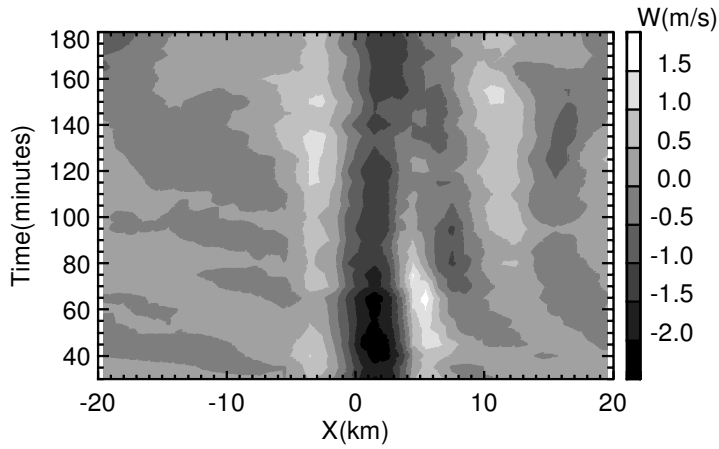

Figure 5. As in Fig. 4(c), but for zero energy input at the surface.

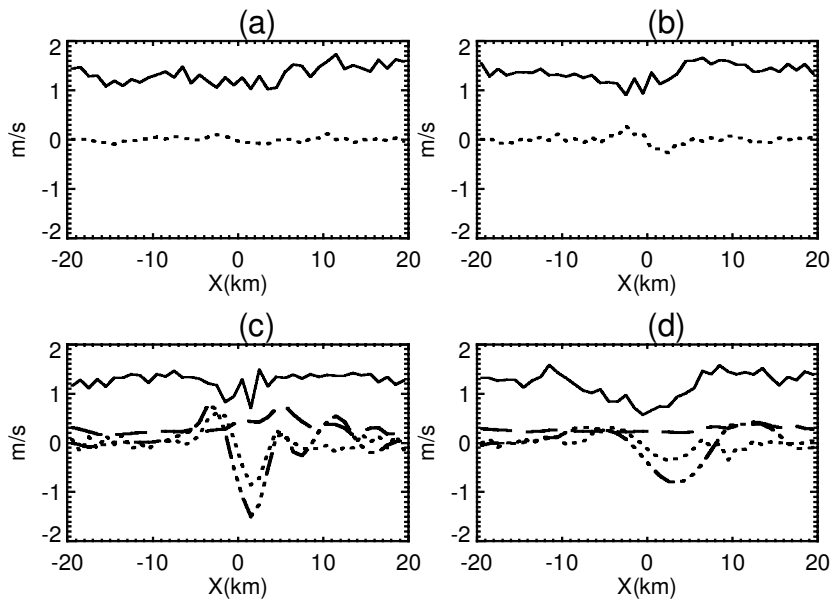

Figure 6. Horizontal distributions of the corresponding mean (dotted line) and standard deviation (solid line) of the vertical-velocity fields illustrated in Fig. 4. Panels (a), (b), (c) and (d) correspond to model configurations A1, A2, A3 and A11, respectively (see text). The corresponding mean (dot-dashed line) and standard deviation (dashed line) of the vertical-velocity fields from simulations A8 and A12 are plotted in (c) and (d), for comparison.

strong descent forced by the wave structure above the hill-summit level is more obvious. On the other hand, vertical motions downstream of the hill, which may be related to lee waves, also exist. Above the CBL the terrain-induced waves are more easy to detect (not shown).

More evidence about these background waves can be seen in Fig. 6, which shows the corresponding mean and standard deviation of the vertical-velocity fields illustrated

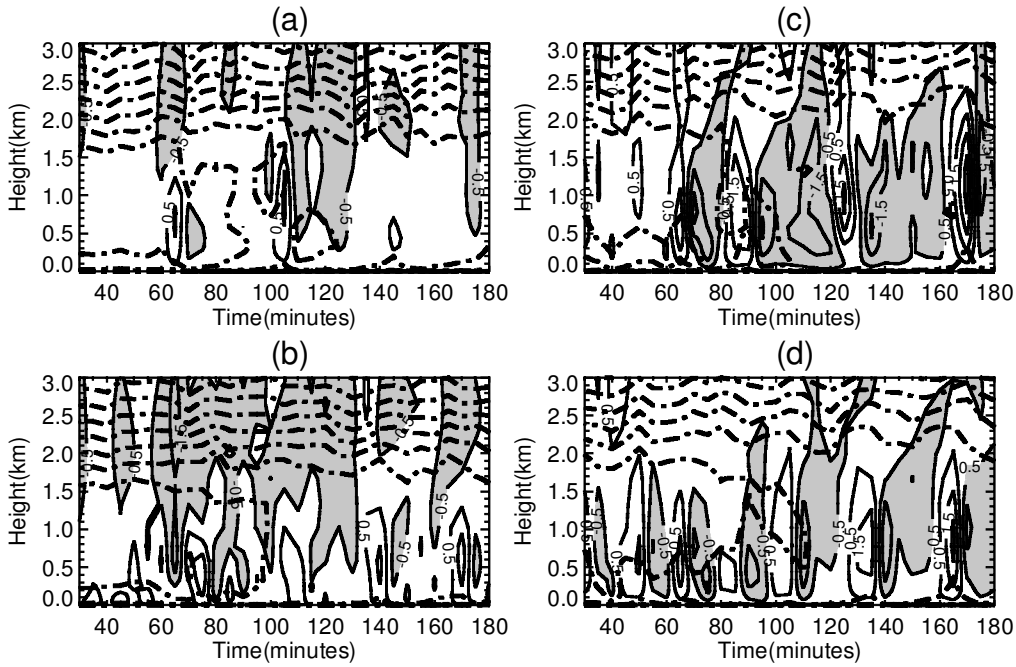

Figure 7. Time–height cross sections of the vertical velocity (a) and (b) at the centre of the model domain and (c) and (d) 10 km downstream of the domain centre. The model configurations are: (a) and (c) A11, and (b) and (d) A3. The corresponding potential-temperature fields are superimposed on each panel for reference (dot-dashed lines).

in Fig. 4. For comparison, the corresponding mean and standard deviation of the vertical-velocity fields from the simulations with model configurations A8 and A12 are also depicted in Fig. 6. The windward slope and downwind slope of the hill are marked by upward motion and downward motion, respectively, as is evident in Figs. 6(b), (c) and (d). The strongest ascent and descent were generated by the hill with a height and width of 500 m and 10 km, respectively, while the largest variability in the horizontal distribution of the standard deviation was associated with a 500 m high and 20 km wide hill. It is also evident in Fig. 6 that the wave amplitudes over and downstream of the hill are large when the surface is not heated, and are diminished when heating is fuelled into the model (see Figs. 6(c) and (d)).

By comparing Figs. 4 and 5, we can see that these steady-state convective eddies are superimposed on background vertical circulation patterns generated dynamically by the terrain. It is interesting that these propagating eddies are significantly affected by strong ascent and descent over the hill, but regain their original properties (see Figs. 4(c) and (d)) once they have passed the hill.

Information about the evolution and vertical structure of an individual convective eddy can be inferred from time–height cross sections at specific sites. Figure 7 shows the time–height cross section of the vertical velocity at a point 10 km downstream and at the centre of the domain. The hill centred in the domain has the same height of 500 m but different widths, i.e. 10 km and 20 km. The time at which convective motion begins to set in is affected by the width of the hill; for smaller widths the convection sets in earlier downstream of the hill. Figure 7 also indicates that the convective eddies downstream of the longer hill appear to have higher strengths and extend deeper in the

vertical while, just above the hill, the eddies have higher strengths for the shorter hill. As a matter of fact, the maximum w is 3.9 m s^{-1} in Fig. 7(c) (the biggest value among these four cases) and 1.9 m s^{-1} in Fig. 7(a) (the smallest among these four cases). The convective eddies are not well defined at the summit of the hill, especially for a longer hill, (Fig. 7(a)), while the convective layer is shallower at the summit than downstream of the hill (although the absolute height of the CBL top is approximately the same).

Careful examination of Fig. 7 indicates that a period of about 30 min can be inferred for the updraughts and downdraughts exhibited in Fig. 7(d), while a slightly longer period of 35 min is suggested in Fig. 7(c). If these eddies move with a speed of 6.6 m s^{-1}, as implied in Fig. 4, the 30 min period suggests a cell spacing of about 12 km for these convective eddies, and the 8 min life cycle implies a cell size of about 3 km. These results confirm the eddy properties exhibited in Fig. 4. The observational study by Raymond and Wilkening (1980) showed that, at lower levels, the heat flux was transferred upwards, primarily via the 3–4 km convective eddies. Although eddy properties may be sensitive to the turbulent scheme and the model resolution used, the bulk characteristics should be less sensitive, as suggested by the test runs discussed in the previous sections.

Figures 4 and 7 also indicate that the effects of the hill on the convection seem to be more pronounced at the initial stage of the model simulation. If the initial stage of the model simulation is regarded as the initial development of the convection, and the final stage of the model simulation is taken as the mature stage, then the mature convective structure is largely governed by the environmental conditions, such as wind speed and surface heat flux, and only weakly disturbed by the hill while, during the initial stage of the convective development, the effects of the hill are more significant. However, it should be pointed out that, during the initial stage, the model adjustment from the 1D initial profile may have also influenced the convection.

(ii) *Eddy vertical-velocity variance characteristics.* To gain more insight into the question of whether hills with different heights and widths have different impacts on the convective properties, the vertical-velocity variance w^2 was examined. Here, we define $\overline{w^2}^t$ as the time-averaged variance obtained by averaging $w^2(x, y, t)$ from the model simulations over the last 60 min. $\overline{w^2}^{t,x}$ and $\overline{w^2}^{t,z}$ are obtained by performing further averaging on $\overline{w^2}^t$ in the x-direction and z-direction, respectively. Figure 8 depicts the corresponding $\overline{w^2}^{t,z}$ and $\overline{w^2}^{t,x}$ for the vertical-velocity fields presented in Fig. 4. It can be noted that the vertical distributions of $\overline{w^2}^{t,x}$ generally have the same character in the CBL for different cases, that is with a maximum in the middle of the mixed layer and minima near surface and above the mixed layer. These vertical distributions of $\overline{w^2}^{t,x}$ are typical of observations of a CBL (Mason and Sykes 1982), but the effects of hill height and width on them are not well pronounced, and the maximum $\overline{w^2}^{t,x}$ is only slightly different for different hills.

One point that needs to be addressed again is that the maximum $\overline{w^2}^t$ over a longer hill is indeed larger than that over a shorter hill of 500 m height. Above the CBL, some differences also exist. When the hill reaches a height of 500 m, the magnitude of $\overline{w^2}^{t,x}$ above the CBL becomes significant. When the hill length is changed to 20 km, the value of $\overline{w^2}^{t,x}$ above the CBL is even larger. The increase in $\overline{w^2}^{t,x}$ above the CBL is related to the gravity waves induced by the hill.

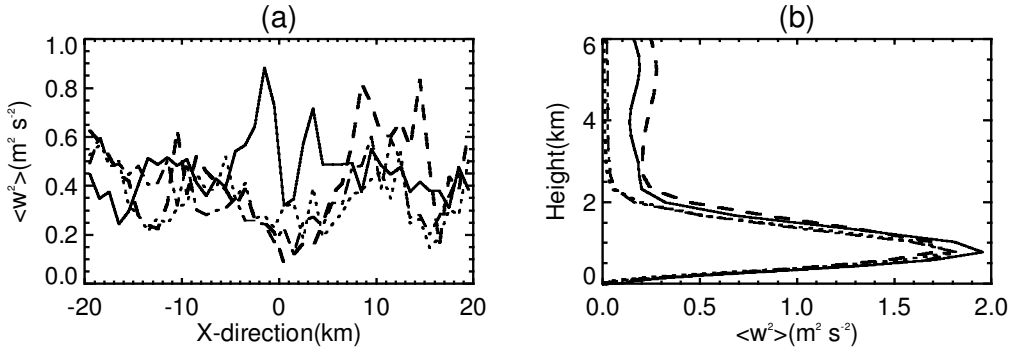

Figure 8. Horizontal and vertical distributions of the time- and space-averaged vertical-velocity variance (a) $\overline{w^2}^{t,z}$ and (b) $\overline{w^2}^{t,x}$ over different hills for simulations with model configurations A1 (dotted lines), A2 (dot-dashed lines), A3 (full lines), and A11 (dashed lines) (see text).

The horizontal distribution of $\overline{w^2}^{t,z}$ is affected by the hill with more complexity than the vertical distribution, as can be seen in Fig. 8(a), and the effects of the hill on $\overline{w^2}^{t,z}$ are different over different regions of the model domain. The strength of eddies at the summit of the hill is much weaker, probably because of the offset effects between the convective eddies and the forced ascent and descent of airflow on either side of the hill (as seen in Fig. 4). This decrease of eddy strength over the hill is more significant when the hill is 500 m high and 20 km wide. However, the strength of eddies downstream of the 500 m high and 20 km wide hill is the strongest. Similarly, it is found that the strength of eddies downstream of the 200 m high and 20 km wide hill is slightly stronger than that for a 200 m high and 10 km wide hill. This further suggests that the length of a relatively high hill has an important impact on the eddy energy distribution, especially downstream. Some hints about this argument can be obtained from the life cycles of the updraughts and downdraughts implied in Figs. 7(b) and (d). The life cycles of the updraughts are generally the same in Figs. 7(c) and (d), i.e. about 8 min on average, but the life cycles for the downdraughts are different. In the case of the longer hill, the descent of the air in the lee persists longer than for the shorter hill. This implies that the surface air has a longer time to accumulate convective energy, leading to higher convective energy and, hence, to fewer but stronger updraughts.

The horizontal distribution of $\overline{w^2}^{t,z}$ in the case of a 500 m high and 10 km wide hill does not agree well with the others, especially, at the summit of the hill. The convective activities upstream and downstream of the 500 m high and 10 km wide hill seem to be more uniformly distributed, while the eddy energy distributions over other hills exhibit a wave-like form with three distinct minima, one just downstream of the summit in the model domain, and four maxima. One possible reason may be that a steep hill may have more significant effects on the small-scale mixing process at lower levels upstream and downstream of the hill. On the other hand, vertical motion dynamically induced by the terrain may affect the energy distribution patterns exhibited in Fig. 8.

To evaluate the potential contributions of the terrain-induced wave energy, and of the energy presented in the forced ascents and descents, to the total vertical-velocity variance (w^2) illustrated in Fig. 8, we simply assume that no interaction exists between the waves and the convective eddies so that the dynamically related energy w_0^2 can be

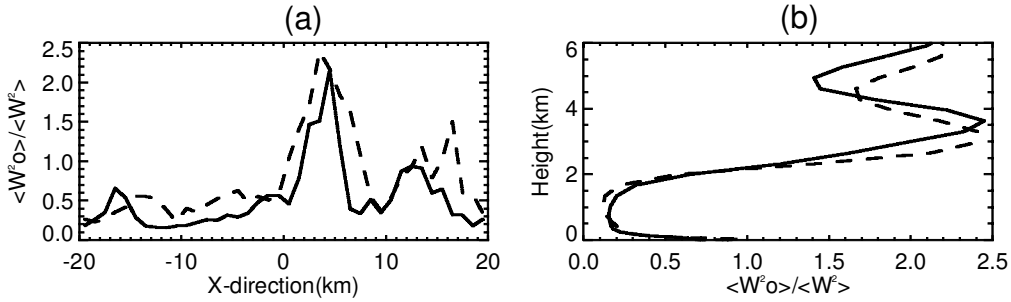

Figure 9. (a) The horizontal distribution of $\overline{w_0^2}^{t,z} / \overline{w^2}^{t,z}$ and (b) the vertical distribution of $\overline{w_0^2}^{t,x} / \overline{w^2}^{t,x}$ evaluated from the simulations A3 and A8 (solid lines), A11 and A12 (dashed lines) (see text).

inferred from the simulations in which no heat flux is fuelled into the model from the surface.

Figure 9 shows the horizontal and vertical distributions of $\overline{w_0^2}^{t,z} / \overline{w^2}^{t,z}$ and $\overline{w_0^2}^{t,x} / \overline{w^2}^{t,x}$ which are obtained from the simulations with model configurations A8 and A12 in association with simulations with model configurations A3 and A11 respectively. It can be seen that $\overline{w_0^2}^{t,z}$ is twice as large as $\overline{w^2}^{t,z}$ just over the downwind slopes of the hills. This again suggests, on one hand, that the offset effects between the convective eddies and the forced descents of airflow over the downwind slope of the hill exist and lead to low $\overline{w^2}^{t,z}$ and, on the other hand, that the forced ascents and descents, which give rise to large $\overline{w_0^2}^{t,z}$ and, hence, large $\overline{w_0^2}^{t,z} / \overline{w^2}^{t,z}$, have a large impact on $\overline{w^2}^{t,z}$ at the summit of the hill. Downstream of the hill, the contribution of the lee-wave energy to the total resolved eddy energy is also significant while, upstream of the hill where the waves are insignificant, $\overline{w_0^2}^{t,z}$ is relatively small compared with $\overline{w^2}^{t,z}$. In fact, both Figs. 6 and 9 suggest that terrain-induced waves seem to be weakened by the convective eddies since the mean profile is relatively unchanged in these simulations. This issue is addressed further in the next section. An examination of the horizontal distribution of $\overline{w_0^2}^{t,z}$ indicates that the horizontal distribution of $\overline{w_0^2}^{t,z} / \overline{w^2}^{t,z}$ is more dependent on $\overline{w_0^2}^{t,z}$ than on $\overline{w^2}^{t,z}$.

The vertical distributions of $\overline{w_0^2}^{t,x} / \overline{w^2}^{t,x}$ show that the dynamic effect of the hills on the total resolved variance (w^2) is relatively small in the mixed layer, while being much larger above the mixed layer. The other feature worthy of emphasizing is that the differences in these vertical distributions corresponding to hills with different widths are not significant in the mixed layer.

(iii) *Effects of buoyancy and evaporative flux.* As we have already seen in Fig. 5, the convective eddies disappear when surface heating is switched off. In fact, the simulation with configuration A7 gives nearly the same results (not shown) to those exhibited in Fig. 5. When configuration A6 is used (i.e. the energy input is increased to 96 W m^{-2}) linear organized convective eddies appear (Fig. 10(a)), although they are still much weaker than the eddies exhibited in Fig. 4, and some of the eddies are so weak that the signals of terrain-induced waves become even more evident. This confirms that energy input into the model from the surface is crucial for the formation of the linear organized

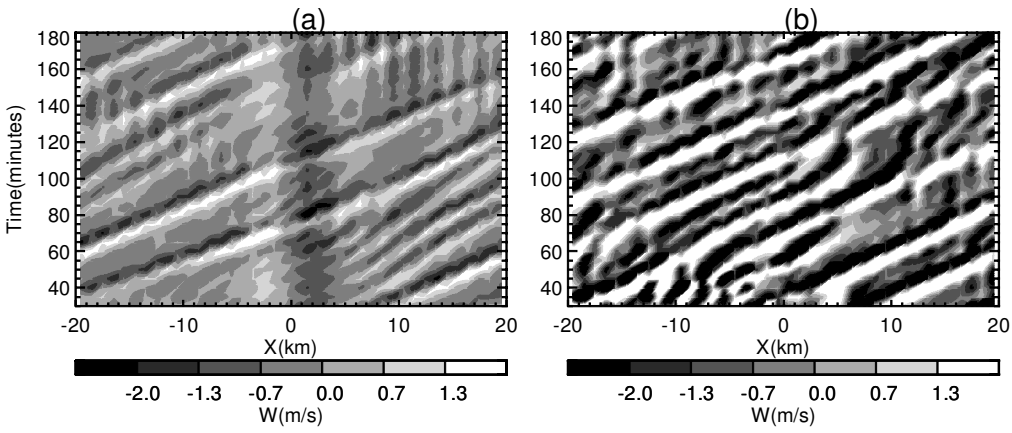

Figure 10. As Fig. 4, but for configurations (a) A6 and (b) A5 (see text).

convective eddies described above. It should be noted that, in our model, the energy input is partitioned into two parts: buoyancy flux and evaporative flux. Configurations A6 and A7 imply that the evaporative flux is essentially turned off by setting $r_s(x)$ to a large value, so that the buoyancy flux equals the energy input. The observational study by Weckwerth *et al.* (1999) also indicated that the formation of horizontal 2D convective rolls was dependent on the magnitude of the buoyancy flux. They showed that horizontal convective rolls formed when the surface buoyancy flux was greater than 50 W m^{-2} for all observed wind speeds. This critical value of surface buoyancy flux for roll formation is much smaller than that suggested in our model simulations. However, one should note that this critical value suggested by the model simulation is rather coarsely determined on the one hand, and may be sensitive to the resolution and turbulent scheme used in the model on the other.

When the buoyancy flux is increased further to 480 W m^{-2}, but the evaporative flux is still switched off, some of the convective eddies are intermittent (Fig. 10(b)) and less weak, while some stronger eddies are still organized and steady. Under such circumstances, the effects of the hill on convective features are not evident; even the forced ascents and descents on both sides of the hill are not visible any more, and the CBL is mostly affected by buoyancy flux.

Figure 11 shows the x–z cross sections of the time-averaged velocity variance $\overline{w^2}^t$ obtained from simulations with model configurations A5, A6 and A8. It is evident that the waves are strong without surface heating (Fig. 11(c)), while the waves disappear when the surface heating is large (Fig. 11(a)). Figure 11 further suggests that surface flux has a large impact on both waves and convection. It also implies that convection tends to weaken terrain-induced waves, as has been mentioned above.

To understand the dependence of the results on evaporative flux and humidity, two runs were designed: one run is based on configuration A4, the other is based on configuration A3, but the initial humidity is twice as that shown in Fig. 1. The results from these two simulations show no significant difference in the convective features when compared with the results from the simulations with configuration A3. The results here suggest that the boundary-layer convective features are not sensitive to surface evaporative flux in the absence of changes in sensible-heat flux or cloud-moisture processes.

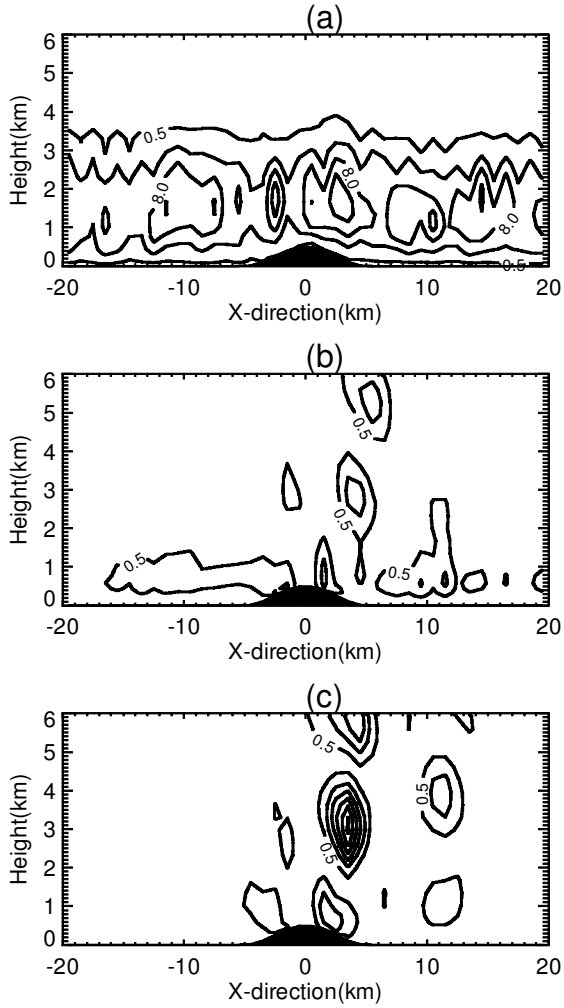

Figure 11. The x–z cross sections of the time-averaged velocity variance $\overline{u^2}^t$ obtained from simulations with model configurations (a) A5, (b) A6 and (c) A8. The averaging period is 120–180 min. The contour intervals in (b) and (c) are 0.5 m^2s^{-2}. The first contour in (a) is 0.5 m^2s^{-2}, and the other contours have an interval of 4 m^2s^{-2}.

(*c*) *Effects of the hill on convective features under light background wind conditions*

(i) *Overall features.* The Hovmöller diagrams of vertical velocities for simulations with model configurations B1, B2 , B3 and B11 are presented in Fig. 12. The convective features in Fig. 12 are quite different from those in Fig. 4. At this stage, an appreciation is necessary of whether the features exhibited in Fig. 12 are related to terrain-induced waves. In fact, with light background winds which remain essentially constant with height, as depicted in Fig. 1, any terrain-induced waves are weak or, at most, appear as a shallow wave with only weak vertical currents. The Hovmöller diagram of vertical velocities from the simulation with model configuration B8 indicates that there are no strong vertical motions over and downstream of the hill (not shown) and, hence, no distinct gravity waves are generated under such circumstances.

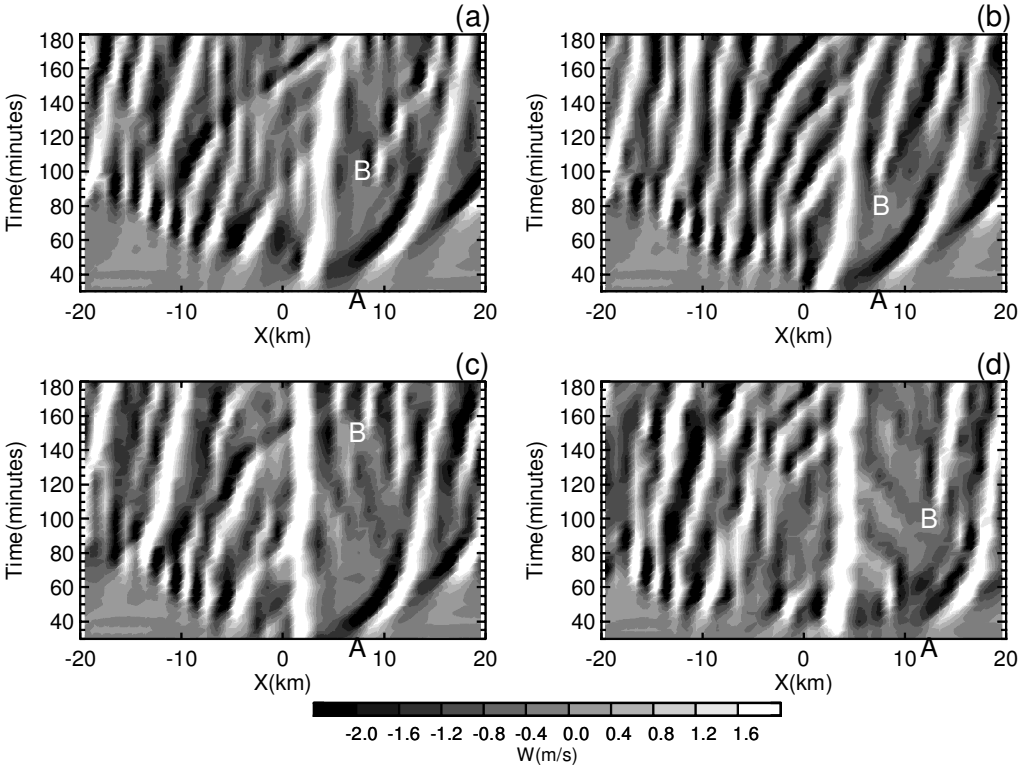

Figure 12. As Fig. 4, but for light-wind conditions. See text for the significance of the letters A and B.

Figure 12 demonstrates that there are more convective cells in the domain than under stronger-wind conditions, but some of these eddies are not steady. These convective eddies are more stationary and less organized under light background winds than those under stronger background winds. Some of the previous observational studies, as well as model simulations, have suggested that there is a minimum wind-speed criterion that must be met before organized boundary-layer convection is formed (e.g. Malkus and Riehl 1964; Weckwerth *et al.* 1997).

The convection downstream of the hill develops more slowly than that upstream while, as we have noted, under stronger background winds convection develops more quickly downstream of the hill. As in Fig. 4, Fig. 12 shows that the convective features for different hills are generally the same, although some slight differences in the cell number and intensity, as well as in the cell steadiness, can be noted between different hills. Figure 12 shows, furthermore, that the convective eddies are first generated near the hill, and then more eddies begin to set in successively both upstream and downstream. Also of interest is that the upward motions seem to be generated continuously just at the foot of the hill (marked by the letter A in each panel of Fig. 12). Once these updraughts are generated, they drift slowly and steadily downstream and, after some time, new updraughts appear at the same place (marked by letter B in each panel of Fig. 12).

Particularly noticeable is the strong and stationary, or slow-moving, updraught at the summit of the hill, or slightly downwind of the peak. Note that the vertical motions at the summit of the hill under stronger-wind conditions are quite weak. It is necessary

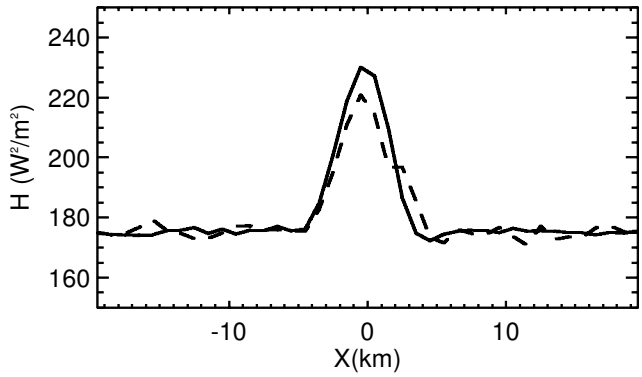

Figure 13. The horizontal distribution of the time-averaged surface buoyancy flux under different background winds (the solid line is for stronger-wind conditions and the dashed line is for light-wind conditions). The averaging period is 120–180 min.

here to make clear again the relative importance of the mechanical as opposed to the thermal forcing of a hill. Figure 13 shows the horizontal distributions of the surface buoyancy flux under different background winds obtained from simulations with model configurations A3 and B3. The surface buoyancy flux increases on the top of the hill due to the lower surface temperature and the consequent decrease of the evaporative flux. It can also be noted that the horizontal distributions of the surface buoyancy flux under different background winds are nearly the same, i.e. the thermal forcing of the hill is independent of the wind conditions. We believe that the thermal effects of the hill under light-wind conditions are dominant, while the mechanical forcing of the hill under stronger background winds is more important in terms of the hill-induced effects on the boundary-layer convective features. Under stronger background winds, the forced ascent and descent over the hill seem to act to suppress the terrain-induced thermal effects, so that although there is significant increase of the surface buoyancy flux over the hill top, no corresponding convective activities can be observed. However, when the background winds are small, the forced ascents and descents are weak and the heat-flux anomaly induced by the hill comes into action. The strong updraughts at the summit, or slightly downwind of the peak, are probably partly caused by this elevated heat-flux anomaly and the consequent baroclinicity.

Observational studies (e.g. Braham and Draginis 1960; Raymond and Wilkening 1980) have shown that, under light winds, a convective core exists over the mountain, or slightly downwind of the peak, in which there are many strong updraughts and downdraughts with a net, but much weaker, upward motion. The strong updraughts exhibited in Fig. 12 may be related to this so-called convective core. In their observations, the ultimate origin of the energy source that drives the eddies is not clear, but their observations did show that large values of the heat flux exist over the mountain range. In the current circumstances, the increase of the surface buoyancy flux over the hill top is due to the decrease of temperature over the hill top.

(ii) *Eddy vertical-velocity variance characteristics.* As in Fig. 8, Fig. 14 shows the corresponding $\overline{w^2}^{t,z}$ and $\overline{w^2}^{t,x}$ for the vertical velocity fields presented in Fig. 12. A comparison between Figs. 14 and 8 indicates that, under light background wind conditions, the differences in the horizontal distributions of $\overline{w^2}^{t,z}$ for different hills

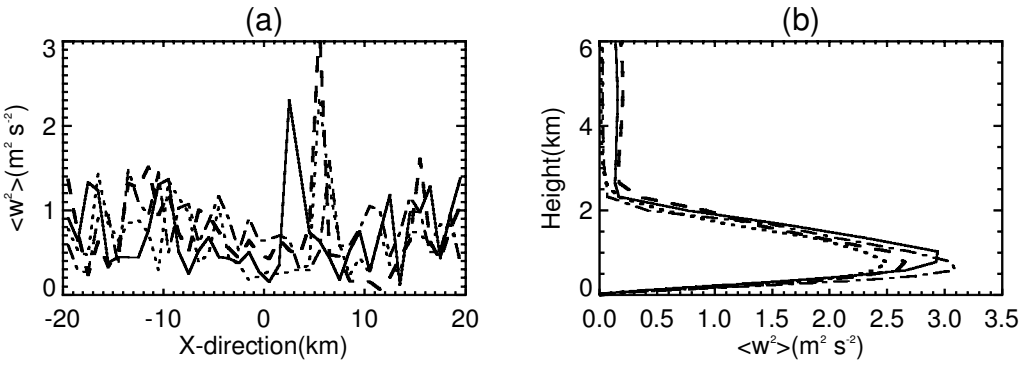

Figure 14. As Fig. 8, but for light-wind conditions.

are not so significant as those under stronger background wind conditions. A well pronounced maximum over the lee slope, which is related to the quasi-stationary upward motions near the centre of the domain (as illustrated in Fig. 12), can be noted in Fig. 14 for all kinds of hill. Also apparent is that $\overline{w^2}^{t,x}$ is much larger than that under stronger background winds.

It can seen from Fig. 14 that the largest $\overline{w^2}^{t,x}$ corresponds to the hill with a height of 200 m while the largest $\overline{w^2}^{t,z}$ is associated with the 500 m high and 20 km wide hill. In the case of the 200 m high and 10 km wide hill, there are more eddies in the domain and the convective core is not clearly defined (see Fig. 12). As a result, $\overline{w^2}^{t,z}$ is smallest over the lee of the hill, but the overall convective activity in the convective layer determined by, say, $\overline{w^2}^{t,x}$ is large. When hill is 500 m high, the convective core is well pronounced and, hence, $\overline{w^2}^{t,z}$ is relatively large. The results here suggest again that the effects of the hill on the convective properties are not simply dependent on the slope of the hill.

The horizontal and vertical distributions of $\overline{w_0^2}^{t,z} / \overline{w^2}^{t,z}$ and $\overline{w_0^2}^{t,x} / \overline{w^2}^{t,x}$, which are identical to those in Fig. 9 but for light-wind conditions (not shown), indicate that $\overline{w_0^2}^{t,z} / \overline{w^2}^{t,z}$ is quite small in the mixed layer and that the fluctuations exhibited in the horizontal distributions of $\overline{w_0^2}^{t,z} / \overline{w^2}^{t,z}$ are mainly caused by the variations of the strength of the thermal eddies. This may further indicate that the gravity waves under light background wind conditions are negligible and that the dynamical effects of the hill on the boundary-layer convection are less important than those under stronger-wind conditions.

As under stronger background wind conditions, the CBL features are largely affected by the surface buoyancy flux under light background winds. However, if the surface buoyancy flux is increased to 480 W m^{-2}, the nearly stationary and strong updraught just over the hill is still quite evident (not shown). This suggests that the effects of the hill on the convection are still significant, even when the surface buoyancy flux is much larger (in contrast to the strong-wind case).

(iii) *Analysis of the convective core.* A careful look at Fig. 12 reveals that the strong updraughts at the summit of the 100 m high and 200 m high hill are less stationary. The Hovmöller diagram of vertical velocity for simulations with model configuration B10 (not shown) also indicates that the strong updraughts at the summit of the 200 m high

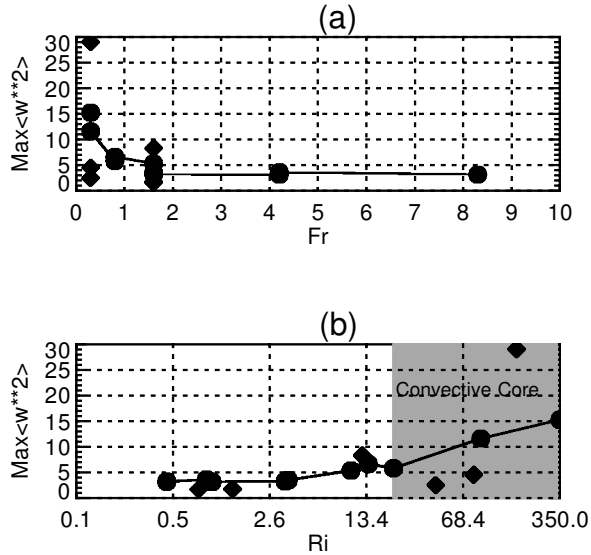

Figure 15. Domain-maximum vertical-velocity variance, from the last two hours of simulations, plotted against (a) the Froude number, *Fr*, based on the background stability, and (b) the Richardson number, *Ri*, based on the surface temperature anomaly, as described in the text. Simulations with surface heat fluxes identical to those in configuration A2 are plotted as circles and those with other heat fluxes as diamonds. In (b) the regime for which a convective core is evident is denoted by shading.

and 20 km wide hill drift downwind of the hill top. One needs to clarify under what circumstances the strong updraughts over a hill remain essentially stationary and form the so-called convective core, rather than drifting away from the hill top.

An important parameter controlling the flow response to the topography is Froude number ($Fr = U/Nh$). Within a convective boundary layer, the value of N is close to zero and the Froude number is not meaningful, but a Froude number based on the stability of the background flow above the boundary layer can be computed. Figure 15(a) shows a decrease in the domain-maximum vertical-velocity variance with this *Fr*, but there is considerable scatter according to simulations with different surface heat fluxes. Use of a background N in the computation of *Fr* is unsatisfactory since we expect the convective eddies to be controlled by CBL processes, and so here we attempt to relate the numerical results to a non-dimensional parameter controlled by the thermal forcing at the surface.

Under light background winds, there are two basic scenarios of flow over hills: when the hill is relatively low with a small slope, the air may flow slowly over the hill and the convective eddies can also drift along with main winds; when the flow approaches a relatively steep hill the bulk properties of the flow may change. Windward of the hill, some portion of the approaching flow may be deflected to form a roll vortex at the hill base while the rest of the flow streams over the hill to form a lee eddy. To demonstrate these kinds of phenomena, Fig. 16 shows the contour plots of the horizontal and vertical velocities averaged over last 30 min of the simulations with model configuration B3. A weak vortex at the windward hill base and a strong lee eddy can be inferred from the horizontal velocity fields, while the convective updraught regions are marked by low-level convergence and upper-level divergence. An examination of the corresponding Hovmöller diagram of horizontal velocity (not shown) indicates that a weak roll vortex at the windward hill base and a strong lee eddy appear

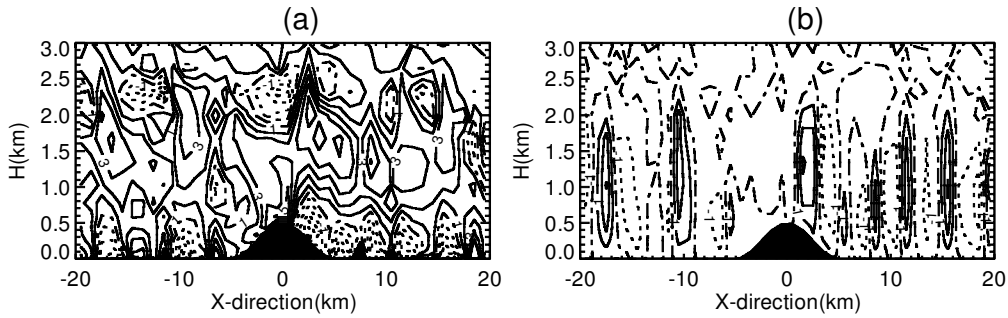

Figure 16. Contour plots of (a) the horizontal velocity and (b) the vertical velocity averaged over last 30 min of the simulations with model configuration B3. The contour interval is 1.0 m s^{-1} and negative contours are dashed.

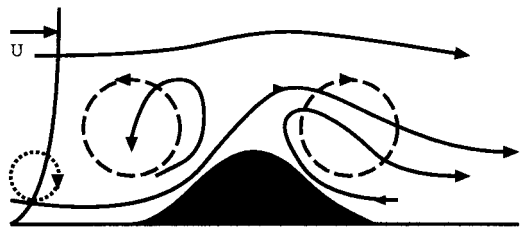

Figure 17. Schematic diagram of the flow pattern illustrated in Fig. 16. The dashed circles represent the baroclinic vorticity tendency and the dotted circle represents the basic-state vorticity.

to exist throughout the simulation. To show this more clearly, a schematic diagram of the flow pattern is given in Fig. 17. We believe that this kind of flow pattern has potential importance with respect to terrain-induced convection and its development.

The underlying process may be interpreted in terms of baroclinic generation of vorticity in the boundary layer (see Fig. 17). The basic-state winds exhibit a positive y-component of vorticity due to the shear of u with height; on the sides of the hill there are baroclinic vorticity generation terms that are negative on the upwind slope and positive on the downwind slope. The combination of these leads to a stronger baroclinic vortex to the lee of the hill and a weaker roll vortex at the windward hill base. The maximum sensible heating at the summit may also contribute to displacing the convective core downstream, as it tends to imply a maximum surface thermal anomaly downstream. These considerations can be analysed by considering the 2D vorticity equation in the y-direction, with the Coriolis effects and the turbulent friction forces neglected:

$$\frac{\partial \xi}{\partial t} = -u\frac{\partial \xi}{\partial x} - w\frac{\partial \xi}{\partial z} - \frac{g}{\theta}\frac{\partial \theta}{\partial x}, \tag{2}$$

where $\xi = \partial u/\partial z - \partial w/\partial x$, θ is potential temperature and g is gravitational acceleration. In a steady-state limit ($\partial \xi/\partial t = 0$) and shallow boundary-layer flow context, the vorticity equation is approximated by

$$u\frac{\partial \xi}{\partial x} = -\frac{g}{\theta}\frac{\partial \theta}{\partial x}. \tag{3}$$

Based on (3), the baroclinic vorticity anomaly $\delta\xi$ can be further approximated by some scaling variables. As we are interested in baroclinic vorticity generation on the scale of the hill, we select a streamline originating at the hill height, so that the horizontal

advective length scale equals the horizontal scale of the baroclinicity between the sloping surface and the well mixed boundary layer, to give,

$$\delta\xi = \frac{g}{\Theta_0}\frac{\delta\theta}{U}, \tag{4}$$

where Θ_0 is the average potential temperature and U is the wind speed in the convective boundary layer, $\delta\theta$ is the departure of potential temperature over the slope, θ_s, from the potential temperature Θ_0. Equation (4) can be non-dimensionalized by dividing by ξ_0, the vorticity due to shear which is proportional to U/h (U being the advection speed and h the hill height and the elevation of the chosen streamline):

$$\frac{\delta\xi}{\xi_0} = \frac{gh}{\Theta_0}\frac{\delta\theta}{U^2}. \tag{5}$$

Note that $Ri = \delta\xi/\xi_0$ is actually a Richardson number. One can see from (5) that the wind speed U may have a large impact on the magnitude of $\delta\xi/\xi_0$. This relation is independent of the hill width; a reduction in the baroclinicity seems to be balanced by an increase in the advection time.

In theory, stationary strong updraughts can be expected over the hill top when the baroclinic vorticity dominates, i.e. $\delta\xi \gg \xi_0$, otherwise, convective eddies tend to be advected away by the main wind. It is, therefore, instructive to assess the Richardson number of different simulations in terms of the occurrence of a clear convective core (deduced from Hovmöller plots such as that of Fig. 12). Figure 15(b) plots the domain-maximum vertical-velocity variance of 16 simulations against Ri, and indicates by shading the cases that exhibit a convective core. From this figure we infer that a critical Ri value for occurrence of the convective core is around 20 to 40. It is apparent that, under stronger-wind conditions, such a value can seldom be reached and, hence, no stationary updraughts occur over the hills.

More implications of (5) can be deduced by considering a state in which baroclinic vorticity generation is balanced exactly by the basic-state vorticity, or $\delta\xi = \xi_0$. In this case, a critical mean convective boundary wind is given by,

$$U_c = k\left[\frac{gh\delta\theta}{\Theta_0}\right]^{\frac{1}{2}}, \tag{6}$$

where k is a constant (note that U_c/U is directly related to the critical Richardson number and can be inferred from Fig. 15(b)). U_c is a measure of the terrain-induced baroclinic circulation. If the basic wind speed $U < U_c$, baroclinic overturning will happen over the hill top with some portion of surface air flow being reversed. Under such conditions, the terrain-induced thermal circulation will play a key role in triggering convection. If the basic wind speed $U \gg U_c$ (i.e. the basic-state shear dominates) the terrain-induced thermal circulation is not important any more, while terrain-related waves may become significant. In this case, the topography will not necessarily act as a trigger of convection; on the contrary, under some circumstances it tends to suppress convection, as we have noted that convective eddies are weak just above the hills. It is worth pointing out again that, under strong background winds, the triggering of convection by topography, if it exists, is only pronounced downstream of orography.

(*d*) *Diagnosis of CAPE and parcel buoyancy*

From the above discussions, we have noted that the strength of eddies at the summit of the hill is weaker under stronger-wind conditions and larger under light-wind

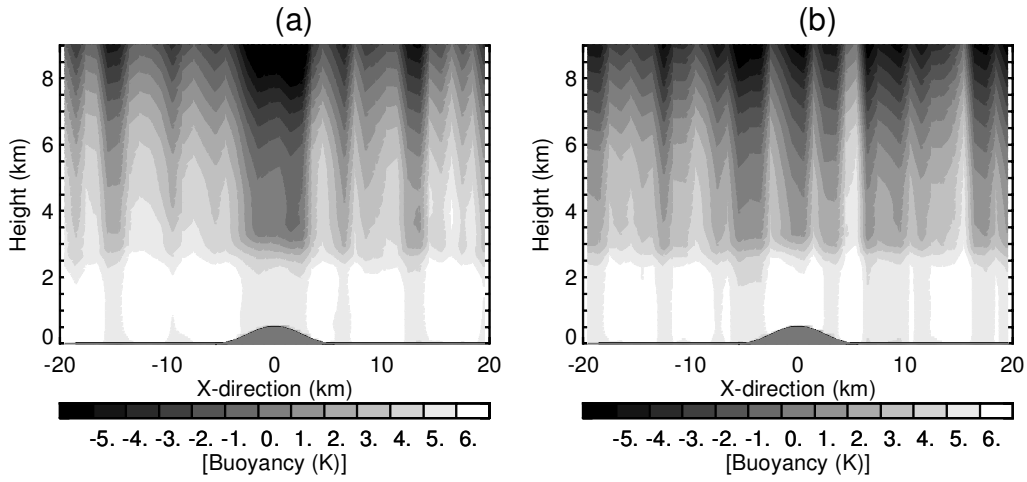

Figure 18. The parcel buoyancy field $T_{vp} - T_{ve}$ (see text for details) calculated from the instantaneous thermal fields (at model simulation time 180 min) from simulations (a) A3 and (b) B3.

conditions, while the eddies downstream of a longer hill are stronger than those of a shorter hill under stronger-wind conditions. In the preceding sections we have related these features to forced ascent and descent and terrain-induced waves. To diagnose the potential effects of hills on moist convection, the CAPE and the buoyancy of the air parcels are examined here. To compute the CAPE, the instantaneous virtual-temperature field from the model simulation is taken as the environment profile, T_{ve}, we only consider air parcels that are lifted from the surface level, and a pseudo-adiabatic process is assumed in calculating parcel virtual temperature T_{vp}.

Figure 18 shows the parcel buoyancy field $T_{vp} - T_{ve}$ calculated from the instantaneous thermal fields gathered at model simulation time 180 min in simulations A3 and B3. One can see that the air parcel is buoyant at the summit of the hill under light-wind conditions, while the air parcel has less buoyancy over the hill when wind speeds are strong. Again, the high-buoyancy area at the summit of the hill, or just downwind of the peak, is related to the convective core.

Figure 19 illustrates the horizontal distributions of the time-averaged CAPE calculated from simulations with model configurations A3, A11, B3 and B11. Two time periods, 30–90 min and 120–180 min, were used for data averaging. Although the CAPE is nearly the same for different hills at the final stage of the model simulation, the differences are evident at the initial stages of model simulations A3 and A11, and the CAPE downstream of the longer hill is, indeed, higher than that of the shorter hill before the boundary-layer convection is fully developed. This may also suggest, on the other hand, that hills may have a potential impact on the convection in the initial stage of convection development. Also noticeable in Fig. 19 is that the CAPE is small at the summit of different hills and reaches its maximum value in the lee of the hills under strong-wind conditions; this is because the eddies over the hill are suppressed and θ_e accumulates in the surface layer in the lee of the hill. Under light-wind conditions, the CAPE just downwind of the top of hills is slightly higher than that elsewhere at the final stage of the simulations.

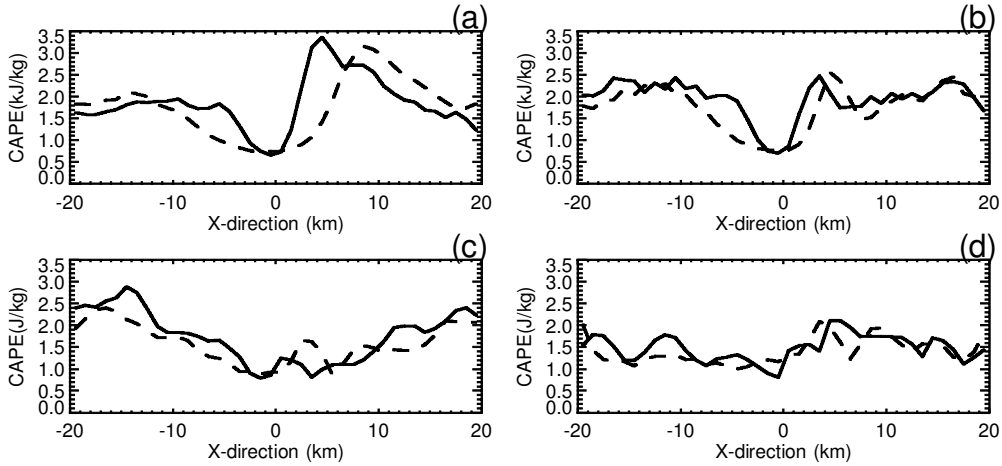

Figure 19. Horizontal distributions of the time-averaged CAPE (see text for details) estimated from simulations. Panels (a) and (b) are for simulations A3 and A11, and (c) and (d) for B3 and B11. The averaging period is shown at the top of each panel. The solid lines correspond to simulations A3 and B3 and the dashed lines correspond to simulations A11 and B11.

5. Remarks and conclusions

There are a number of physical mechanisms that have been found to be important in modulating the resolved eddies and the mean state in these simulations. These include the various effects of hill-induced gravity-wave motion in the stable layer above the CBL, thermal-forcing anomalies on the elevated surface due to decreasing evaporation with temperature, and baroclinic forcing as a result of elevated heating.

It has been found that there is exclusion between the gravity waves and the convective eddies. The vertical forcing due to gravity waves tends to suppress eddy activity; in particular, forced descent in the lee of the hill can allow anomalously warm air to accumulate near the surface, leading to more intense eddies just downstream. Conversely, intense convection tends to reduce the strength of the gravity-wave signal above the hill. The eddy details, such as eddy size, eddy spacing and eddy propagation speed, may be sensitive to the resolution and the turbulence scheme used in the model simulation, but the overall features are more general.

The combined effect of a sensible-heating maximum on the hill summit and baroclinic tendencies due to the elevated heating are a tendency to produce a convective core under reasonably light-wind conditions. The combination of these leads to a stronger baroclinic vortex in the lee of the hill and a tendency for the convective core to be displaced slightly downstream. It appears that we can categorize this phenomenon in terms of a critical Richardson number.

In the triggering of moist convection by hills, it is possible to identify three potential mechanisms: forced lifting, elevated heating and local surface moisture anomalies. This study has demonstrated that, for hills shallower than the CBL depth, forced lifting is not significant because the absolute CBL depth is not strongly modified by the hill. However, wave activity over such a hill may lead to more intense convective eddies in the lee. In regard to the effects of elevated heating, a strong convective core may develop just downwind of the summit in a region of enhanced parcel buoyancy, provided that the mean winds are light.

The major boundary-layer convective features from the simulations performed in this study are as following:

Under stronger-wind conditions

- Eddies are first generated downstream of the hill;
- Steady-state eddies are organized and propagate steadily along the main wind direction;
- The hill tends to weaken convective activities at its summit because of the strong induced descents. The absolute depth of the CBL at the summit of the hill is less than that downstream and upstream, but the altitude above mean sea level remains approximately constant;
- Gravity waves have significant effects on the eddy strength, while convective eddies tend to weaken these waves;
- The strength of the convective eddies downstream of the hill increases with the hill length. However, the effects of the hill length on the results are only significant when the height of the hill reaches 500 m;
- The air parcel has less buoyancy and the CAPE is smaller at the summit of the hill.

Under light-wind conditions

- Eddies are less organized and more stationary;
- Eddies develop more quickly upstream of the hill, and there are more eddies upstream of the hill than downstream;
- Eddy strength is stronger than that under higher-wind conditions. As in the case of stronger background winds, a longer hill has more significant effects on the boundary-layer convective features, given that the hill is not too low to force any differences;
- Strong updraughts can be observed at the summit of the hill, or slightly downwind of the peak, and we link these with a so-called convective core;
- The thermal effects of a hill on the eddy behaviour are thought to be important. The elevated buoyancy fluxes over the hill are likely to serve as an energy support for the so-called convective core;
- An air parcel has more buoyancy at the summit of the hill and the CAPE downwind of the top of hills is slightly higher than that elsewhere.

It is important to recognize here that the enhancement of the convective activity downstream of the hill under strong background winds, and the strong updraughts at the summit of the hill under light winds, have potential implications for the triggering of deep convective systems when cloud processes and conditional instability are present. Also of importance is an understanding of how and to what extent the hills affect the accumulation and release of CAPE, which is thought to be fundamental for the formation of the deep convective systems. It is possible that these processes may differ in the case of an isolated (or 3D) hill, in which case significant influence on the downstream flow may be possible over distances greater than the horizontal periodicity of the model used here. Such studies are currently being made.

ACKNOWLEDGEMENTS

Wen-Shou Tian has been supported by an Overseas Research Scholarship during the progress of this work. Simon Vosper has provided many useful comments on the results and the manuscript.

REFERENCES

Bader, D. C. and McKee, T. B. 1991 Mesoscale boundary-layer evolution over complex terrain. Part II: Factors controlling nocturnal boundary-layer structure. *Mon. Weather Rev.*, **120,** 802–816

Bader, D. C., McKee, T. B. and Tripoli, G. J. 1987 Mesoscale boundary-layer evolution over complex terrain. Part I: Numerical simulation of the diurnal cycle. *J. Atmos. Sci.*, **44,** 2823–2838

Braham, R. R. and Dragins, M. 1960 Roots of orographic cumuli. *J. Meteorol.*, **17,** 214–226

Clark, T. L. 1977 A small-scale dynamic model using a terrain-following transformation. *J. Comp. Phys.*, **24,** 186–215

Deardorff, J. W. 1977 Three-dimensional numerical study of the height and mean structure of a heated planetary boundary layer. *Boundary-Layer Meteorol.*, **7,** 81–106

Gopalakrishnan, S. G., Roy, S. B. and Avissar, R. 2000 An evaluation of the scale at which topographical features affect the convective boundary layer using large eddy simulations. *J. Atmos. Sci.*, **57,** 334–351

Hewer, F. E. 1998 Non-linear numerical model predictions of flow over an isolated hill of moderate slope. *Boundary-Layer Meteorol.*, **87,** 381–408

Huntingford, C., Blyth, E. M., Wood, N., Hewer, F. E. and Grant, A. 1998 The effect of orography on evaporation. *Boundary-Layer Meteorol.*, **86,** 487–504

LeMone, M. A. 1973 The structure and dynamics of horizontal roll vortices in the planetary boundary layer. *J. Atmos. Sci.*, **30,** 1077–1091

Malkus, J. S. and Riehl, H. 1964 Cloud structure and distributions over the tropical Pacific Ocean. *Tellus*, **16,** 275–287

Martin, D. W. and Schreiner, A. J. 1981 Characteristics of west African and east Atlantic cloud clusters: A survey from GATE. *Mon. Weather Rev.*, **109,** 1671–1688

Mason, P. J. and Sykes, R. I. 1982 A two-dimensional numerical study of horizontal roll vortices in an inversion capped planetary boundary layer. *Q. J. R. Meteorol. Soc.*, **108,** 801–823

McNider, R. T. and Pielke, R. A. 1981 Diurnal boundary-layer development over sloping terrain. *J. Atmos. Sci.*, **38,** 2198–2212

Moeng, C. H. and Sullivan, P. P. 1994 A comparison of shear and buoyancy driven planetary boundary layer flows. *J. Atmos. Sci.*, **51,** 999–1022

Raymond, D. and Wilkening, M. 1980 Mountain-induced convection under fair weather conditions. *J. Atmos. Sci.*, **37,** 2693–2706

Rowell, D. P. and Milford, J. R. 1993 On the generation of African squall lines. *J. Climate*, **6,** 1181–1193

Schadler, G. 1990 Triggering of atmospheric circulations by moisture inhomogeneities of the earth's surface, *Boundary-Layer Meteorol.*, **51,** 1–29

Tripoli, G. J. and Cotton, W. R. 1988 A numerical investigation of an orogenic mesoscale convective system. Part 2: Analysis of governing dynamics. *Mon. Weather Rev.*, **103,** 406–419

1989 Numerical study of an observed orogenic mesoscale convective system. Part 1: Simulated genesis and comparison with observations. *Mon. Weather Rev.*, **117,** 272–304

Walko, R. L., Cotton, W. R. and Pielke, R. A. 1992 Large-eddy simulations of the effects of hilly terrain on the convective boundary layer. *Boundary-Layer Meteorol.*, **58,** 133–150

Weckwerth, T. M., Wilson, J. W., Wakimoto, R. M. and Crook, N. A. 1997 Horizontal convective rolls: Determining the environmental conditions supporting their existence and characteristics. *Mon. Weather Rev.*, **125,** 505–526

Weckwerth, T. M., Horst, T. W. and Wilson, J. W. 1999 An observational study of the evolution of horizontal convective rolls. *Mon. Weather Rev.*, **127,** 2160–2179

Wood, N. 1995 The onset of separation in neutral, turbulent flow over hills, *Boundary-Layer Meteorol.*, **76,** 137–164

Wood, N. and Mason, P. 1991 The influence of static stability on the effective roughness length for momentum and heat transfer. *Q. J. R. Meteorol. Soc.*, **117,** 1025–1056

1993 The pressure force induced by neutral turbulent flow over hills. *Q. J. R. Meteorol. Soc.*, **119,** 1233–1267